

Cite this: *Mater. Horiz.*, 2019,  
6, 405Received 5th September 2018,  
Accepted 13th November 2018

DOI: 10.1039/c8mh01092g

rsc.li/materials-horizons

## Facile emission color tuning and circularly polarized light generation of single luminogen in engineering robust forms†

Yanhua Cheng,<sup>ab</sup> Shunjie Liu,<sup>ade</sup> Fengyan Song,<sup>ade</sup> Michidmaa Khorloo,<sup>ade</sup>  
Haoke Zhang,<sup>ade</sup> Ryan T. K. Kwok,<sup>ade</sup> Jacky W. Y. Lam,<sup>ade</sup> Zikai He<sup>id\*ac</sup> and  
Ben Zhong Tang<sup>\*ade</sup>

Controlling molecular assembled structures of a single luminogen through external manipulation is a general and powerful concept for designing emission-tunable materials. However, these reported powder-like compounds generally show limited emission color, high serendipitous-discovery dependence and poor mechanical properties. To overcome these limitations, we describe a simple yet powerful strategy that is adapted from methods used to control bulk commodity polymers, to modulate the molecular assembled architecture of dopant. We use luminogens with aggregation-induced emission characteristics and intrinsic blue and yellow emissions at their crystalline and amorphous states as demonstrations. When incorporating such luminogens (AIEgens) in the desired polymer matrix with tailored microstructure, white light and white circularly polarized light are generated, which are inaccessible from single and achiral AIEgen alone. The introduced strategy for realizing diverse light emission is an innovative way of developing luminogens and provides useful continuous emissive materials in the forms of macroscopic films and fibers for developing flexible devices and wearable systems.

### Conceptual insights

Aggregation-induced emission luminogens (AIEgens) are generally characterized by propeller-shaped structures. Such highly twisted conformation coupled with multiple intermolecular interactions allow them to take facile rearrangement of the molecular packing, resulting in distinct variation in photophysical properties. Different from the previous work that focused on molecular-level structural modification, this concept provides success in tuning the packing modes of AIEgens by assembling them with polymers. By engineering the microstructure of polymer hosts, the emission properties of these embedded AIEgens in terms of color and chirality can be fine-tuned accordingly. AIEgens with intrinsic blue and yellow emission in their crystalline and amorphous states are chosen as a demonstration. Combining the interactions between AIEgens and polymer chains as well as the polymeric internal helical-structure control, white emission and white circularly polarized light (CPL) are achieved in polymer composites that are inaccessible from single and achiral AIEgens alone. This work not only opens up new design of AIEgen-assembled materials for versatile emission tuning, but also provides a new concept of exploiting new luminescent materials that are mechanical flexible and compliant to integrate with wearable systems.

## Introduction

Luminescent materials with tunable optical properties continue to fascinate mankind owing to their potential applications in various fields.<sup>1,2</sup> Integration of these materials with textiles or biological tissues is of great interest in wearable systems and biomedical areas.<sup>3–6</sup> Their unique requirements are that they should be flexible to survive mechanical deformation and be mechanically compliant with arbitrary surfaces or movable parts to undergo bending and stretching.<sup>6–8</sup> Advanced synthetic methodologies developed at the molecular level have been extensively used to produce such polymeric materials with tunable emission properties, such as intensity, color, and polarization.<sup>9,10</sup> Versatile and controllable methodologies to produce these materials are still highly desirable but remain challenging.

Nature provides drastically facile strategies that enable the soft skins of animals to display versatile colors and/or luminescence,<sup>11,12</sup> which combine chromophores and biopolymers

<sup>a</sup> Department of Chemistry, The Hong Kong Branch of Chinese National Engineering Research Center for Tissue Restoration and Reconstruction, Institute for Advanced Study and Development of Chemical and Biological Engineering, The Hong Kong University of Science and Technology, Clear Water Bay, Kowloon, Hong Kong, China. E-mail: tangbenz@ust.hk

<sup>b</sup> State Key Laboratory for Modification of Chemical Fibers and Polymer Materials, College of Materials Science and Engineering, Donghua University, Shanghai, 201620, China

<sup>c</sup> School of Science, Harbin Institute of Technology, Shenzhen, HIT Campus of University Town, Shenzhen, 518055, China. E-mail: hezikai@hit.edu.cn

<sup>d</sup> HKUST-Shenzhen Research Institute, No. 9 Yuexing 1st RD, South Area, Hi-tech Park, Nanshan, Shenzhen 518057, China

<sup>e</sup> Center for Aggregation-Induced Emission, SCUT-HKUST Joint Research Institute, State Key Laboratory of Luminescent Materials and Devices, South China University of Technology, Guangzhou, China

† Electronic supplementary information (ESI) available: Materials and methods, fabrication procedures, characterizations. See DOI: 10.1039/c8mh01092g

into micro-structured composites to elicit sophisticated functionalities. Such synergic effect can be illustrated by the tunable skin color of cephalopods and the circularly polarized luminescence (CPL) of fireflies.<sup>13</sup> Inspired by these versatile strategies together with the vast array of new chromophores, extensive color-tunable polymer composites have been developed, where the emission color variation is associated with the structural modification of the molecular assemblies in the continuous polymers.<sup>14–16</sup> For example, luminescent molecules based on oligo(*p*-phenylene vinylene) are widely used, which are planar conjugated molecules that readily form co-facial aggregates through  $\pi$ - $\pi$  interactions.<sup>17,18</sup> These aggregates show an excimer fluorescence, different from the monomeric species.<sup>19</sup> Based on the excimer formation and dissolution, the composite materials display tunable monomer/excimer emission. However, owing to the planar structure and strong interfacial interactions, large tensile deformation ( $\sim 200$ – $300\%$ )<sup>20,21</sup> or high temperature treatment<sup>22</sup> are normally required to dissolve its aggregates when blending with the polymer matrix. Therefore, developing new luminescent materials with easy modulation under external manipulation would be awarding.

A promising candidate is the aggregation-induced emission luminogens (AIEgens). Their highly twisted propeller-like conformation coupled with multiple weak intermolecular interactions allow AIEgens to show facile phase transition and variable emissions in the solid state.<sup>23</sup> Distinct emission shifts of up to 100 nm have been reported from crystalline to amorphous state.<sup>24–26</sup> It is believed that in the crystalline phase the molecules take a more twisted conformation to fit into the crystal lattice, while in the amorphous state the molecules assume a more planar conformation to show the red-shifted photoluminescence (PL).<sup>27</sup> Assembling such AIEgens into a polymer matrix with a controlled microstructure<sup>28,29</sup> will provide a versatile platform to endow such distinct polymorphism-dependent AIEgens with tunable and controllable emission color.

Moreover, if these polymer composites can be engineered to emit CPL at the same time, they could ultimately generate a breakthrough in color-image projection and 3D displays.<sup>30</sup> Chirality is often introduced by either connecting chiral moieties through covalent bonds or inheriting from chiral helically assembled structures.<sup>31,32</sup> Alternatively, it has also been demonstrated that CPL can also be generated when unpolarized light propagates through a chiral organization.<sup>33</sup> Benefitting from the significant advancements in polymer materials and technology, we envision that the use of engineered helical microstructures of polymer hosts will enable CPL generation.<sup>34,35</sup> Take advantage of the high sensitivity of AIEgen emission to the external microenvironment and the tailorable design of the host microstructure, polymer composite materials with versatile emissions based on single AIEgen can be anticipated.

Herein, we propose a strategy to endow single and achiral AIEgens with the properties of tunable emission color and CPL based on polymer microstructure control. AIEgens with intrinsic blue and yellow emissions at their crystalline and amorphous states were chosen as a demonstration. When embedding such a single AIEgen into a polymer matrix with an engineered

microstructure, the crystalline and amorphous nano-aggregates of the AIEgen serve as “nano-blocks” and are directed to pack in a specific manner. Specifically, the emission color can be tuned by controlling the amount of crystalline and amorphous “nano-blocks” in the rigid-soft binary polymers. At the same time, single-molecule-based white light emissive materials were also achieved, which can be processed into films and fibers with hierarchical structures as well as white lighting buildings with 1D, 2D and 3D architectures when integrated with UV LED devices. Particularly, white CPL can be generated by further introducing a helical microstructure into the polymer host. These demonstrations are all realized in the forms of macroscopic films and fibers and thus are expected to have broad relevance in flexible and stretchable electronics.

## Results and discussion

### Preparation of emissive polymer composites

To demonstrate the proposal, two butterfly-shaped AIEgens with distinct polymorphism-dependent emission properties were used (Fig. S1 and Table S2, ESI<sup>†</sup>), namely 9,10-bis(di-4'-methylphenylmethylene)-9,10-dihydroanthracene (TDHA) and 9,10-bis(diphenylmethylene)-9,10-dihydroanthracene (PDHA). Their chemical structures are shown in Fig. 1a and b. Taking TDHA for example, crystals of TDHA (abbreviated as TDHA-c) emit blue light with emission maximum ( $\lambda_{\text{max}}$ ) at 425 nm, while their amorphous counterparts (abbreviated as TDHA-am) show a  $\lambda_{\text{max}}$  in the yellow region at 530 nm (Fig. 1c). Because of the free rotation of each group of AIEgens in amorphous states, they show different conformations and each conformer exhibits different electronic energy levels.<sup>36</sup> Therefore, the broader emission bandwidths of the amorphous states than of the crystalline states can be clearly observed (Fig. 1c). It is noted that the emission color of the two aggregates is complementary and white emission may be generated at an appropriate composition in principle.<sup>37</sup> Similarly, the amorphous aggregates of PDHA (abbreviated as PDHA-am) also emit in the redder region than their crystalline counterparts (abbreviated as PDHA-c, Fig. 1d). It is noteworthy that PDHA-am gradually converts to PDHA-c owing to the good self-recovering or fast crystallization ability of PDHA.<sup>26</sup>

It is well-known that the aggregation architectures of AIEgens are sensitive to the rigidity of the surrounding environment.<sup>38</sup> Therefore, commercially available brittle polystyrene (PS,  $T_g = 89$  °C) and rubbery polybutadiene (PB,  $T_g = -50$  °C) as representative rigid and soft matrices were used to control the surrounding environments of AIEgens (Fig. S2, ESI<sup>†</sup>). When TDHA is embedded into PB, the resulting composited thin-film (T-PB) emits a blue fluorescence at  $\sim 430$  nm (Fig. 1c). Such an emission behavior is similar to that of TDHA crystals.<sup>26</sup> When TDHA is assembled with PS, the obtained AIEgen-loaded polymer film (T-PS) exhibits a redder emission at  $\sim 490$  nm. This suggests the existence of both crystalline and amorphous aggregates of TDHA. The free volume in the PS network may allow the TDHA molecules to undergo self-recovery to form

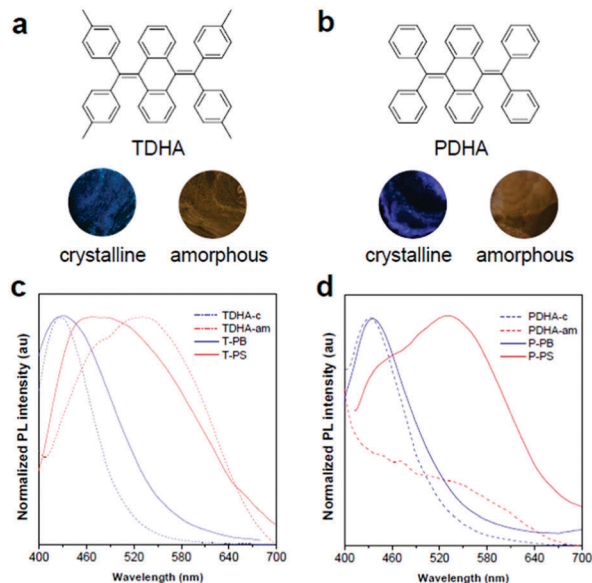


**Fig. 1** Molecular structures of AIEgens studied in this work and their polymorphism-dependent emission behavior. (a and b) Chemical structures of (a) TDHA and (b) PDHA and their fluorescent images of crystalline and amorphous aggregates. (c and d) PL spectra of crystalline and amorphous aggregates of (c) TDHA and (d) PDHA; and (c) TDHA- and (d) PDHA-embedded PB (T-PB and P-PB) and PS (T-PS and P-PS).

crystalline aggregates, whose emission overlaps with that of amorphous ones and generates a broad peak centered at  $\sim 490$  nm.<sup>39</sup> The PL decay curves of the composite films measured at 430 nm and 530 nm further verify the emission stemming from the proposed molecular architectures of TDHA in the PB (Fig. S3, ESI<sup>†</sup>) and PS matrices (Fig. S4, ESI<sup>†</sup>). These results in Fig. 1c and d show that the PB and PS matrices do indeed act as microenvironments to stabilize the crystalline and amorphous species of AIEgens, respectively.

### Color-tunable emission

To achieve a broader color range modulation, the above TDHA-embedded PS and PB matrices are blended in different mass fractions. Owing to the immiscibility of these two polymers, a clear spatial distribution of phase-separated morphology was visualized in the PB/PS films using a fluorescent microscope (Fig. 2a). The change of the two-phase structure by increasing the PS fraction ( $\phi(\text{PS})$ ) was monitored and is shown in Fig. 2a. At  $\phi(\text{PS}) \leq 60\%$ , spherical inclusions of PS are observed in the PS matrix (Fig. S5, ESI<sup>†</sup>). At  $\phi(\text{PS}) = 70\%$ , the pattern shows interpenetrating, continuously extending domains. At  $\phi(\text{PS}) \geq 80\%$ , the phase was reversed and the PS constitutes the matrix.<sup>40</sup> Meanwhile, the resulting image shows a gradual red-shift in the emission color when the fraction of PS is increased in the polymer blend. The PL process of the AIEgens in the polymer matrix is schematically illustrated in Fig. 2b. These results indicate that the crystalline and amorphous AIE assemblies locked in the rubbery and glassy matrices function as nano-blocks to tune the emission color of the polymer blend.

The fluorescence properties of the polymer blend films are further studied by PL spectroscopy. Fig. 3a shows the normalized

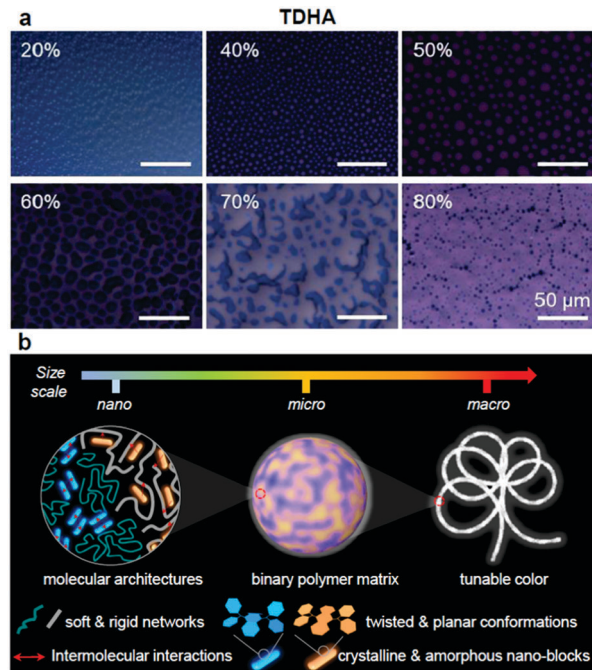


**Fig. 2** Fluorescence color-tuning process. (a) Morphological revolution of microphase separation of PB/PS blends doped with TDHA with increasing mass fraction of PS ( $\phi(\text{PS})$ ). The images were taken on a fluorescent microscope under UV light irradiation. (b) Schematic illustration of the fluorescence color-tuning process by changing the polymer network rigidity to afford AIE crystalline and amorphous nano-blocks in desired compositions.

PL spectra of the TDHA in PS/PB films with  $\phi(\text{PS})$  varying from 10% to 90%. With an increase of  $\phi(\text{PS})$ , the emission peak in the blue region decreases gradually, while the yellow emission becomes stronger accordingly. When the above emission change was transformed into CIE chromaticity coordinates (Table S3, ESI<sup>†</sup>), several new emission colors were found to generate from the polymer blends. A straight line with a nearly perfect correlation coefficient (0.999) can be drawn across all the points of CIE chromaticity coordinates (Fig. S6, ESI<sup>†</sup>) and from point i (0.18, 0.17) to point ii (0.28, 0.35) in the CIE-1931 chromaticity diagram as shown in Fig. 3b. It is worth noting that the above straight line falls into the white region at  $\phi(\text{PS}) \geq 30\%$ . Thus, these results demonstrate that such an approach is a promising methodology to prepare white light-emitting materials based on a single AIEgen. This strategy is also applicable for PDHA to achieve multi-emission by controlling the rigidity of the polymer matrix. As mentioned before, it is difficult to obtain PDHA-am but when PDHA is incorporated in the glassy network of PS, besides a small peak associated with the emission of PDHA-c observed at  $\sim 440$  nm in the PL spectrum of the resulting composite, a new broad peak attributed to the emission of amorphous PDHA (PDHA-am) also appeared at  $\sim 530$  nm (Fig. 1d). The appearance of a broad emission at  $\sim 530$  nm suggests that the metastable PDHA-am could be transformed into a thermodynamically stable state using a glassy PS matrix. Similar to TDHA, the multicolor emission of PDHA can be controlled by changing the fraction

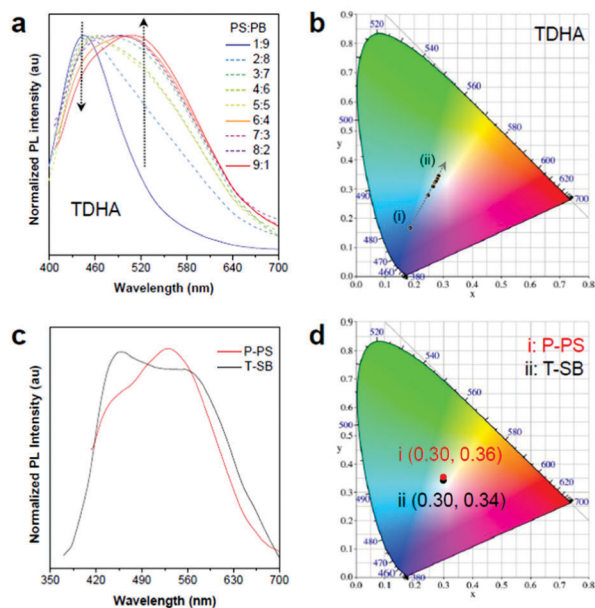


**Fig. 3** Tunable emission color in polymer matrix. (a) Normalized PL spectra of TDHA-doped PB/PS thin films with different  $\phi(\text{PS})$ . The excitation wavelength was 370 nm. (b) Corresponding CIE 1931 coordinates in CIE-1931 chromaticity diagram of TDHA-doped PB/PS samples. (c) Normalized PL spectra of P-PS and T-SB. (d) CIE 1931 coordinates of white emissive P-PS and T-SB in CIE-1931 chromaticity diagram.

ratio of the PB/PS blends (Fig. S7, ESI<sup>†</sup>). In addition, white emission was also obtained at  $\phi(\text{PS}) \geq 60\%$ . The above results show that by rationally choosing an appropriate polymer matrix, several new emission colors, including white color, beyond those of the crystalline and amorphous AIEgens can be achieved.

The interactions between the AIEgens and the polymer matrix play a vital role in controlling the luminescence ratios of the crystalline and amorphous AIEgen nano-blocks. On one hand, the rigidity of the polymer matrix modulates the molecular conformations through free-space control. Similar to the mechanism of polymorphism-dependent emission, the polymer microenvironment with high rigidity restrains the intramolecular rotation and pushes the AIEgens to show planar conformation, while the soft polymer network allows the AIE molecules to move freely to maintain the preferred twisted conformation. It is noteworthy that controlling the rigidity of the polymer matrix is much easier than modulating the morphology of solid-state molecules, which requires sophisticated techniques. On the other hand, the type of intermolecular interactions can manipulate the location of the crystalline and amorphous AIEgen nano-blocks. In PS composites, the abundant intermolecular interactions, arising from phenyl groups of PS and AIEgens, can compete with self-crystallization and isolate AIEgen in the free amorphous state. In PB composites, the lack of phenyl groups in the polymer host weakens the interactions with AIEgens, which readily form crystalline nano-blocks together.

### White emissive materials

Solid-state white organic light-emitting materials and devices play important roles in lighting and displays.<sup>41</sup> The CIE

chromaticity coordinates of (0.33, 0.33) represent a pure white color.<sup>37</sup> From the above results, it was found that the emission of PDHA embedded in a pure PS network (abbreviated as P-PS) is quite close to pure white color with CIE coordinates of (0.30, 0.36) (Fig. 3c and d). For TDHA, a copolymer (SB) of styrene (S, rigid species) and butadiene (B, soft species) is chosen to generate pure white color. Fig. 3c shows the PL of the SB film with TDHA (abbreviated as T-SB). Dual emission bands derived from the rigid and soft segments of SB are observed in the spectrum. The CIE chromaticity coordinates of T-SB were calculated from its PL spectrum and were equal to (0.30, 0.34) (Fig. 3d).

The above white light-emitting polymeric materials combine the fluorescence properties of AIEgens and the mechanics of polymeric materials with good processability, which enable them to form tough films readily or coat directly on any surface in varied geometrical forms to meet different applications. As an example, a transparent and flexible film of P-PS was formed by drop-casting of its solution followed by integration into a 365 nm UV LED, as shown in Fig. 4a. Another example uses a concentrated solution P-PS to paint on arbitrary surfaces, such as optical fibers, as shown in Fig. 4b. When the UV LED is connected to the electrical power, the film-coated LED emits bright white color (Fig. 4c(ii)), while the uncoated one shows only blue emission (Fig. 4c(i)). Similarly, P-PS can be coated on a transparent, flexible

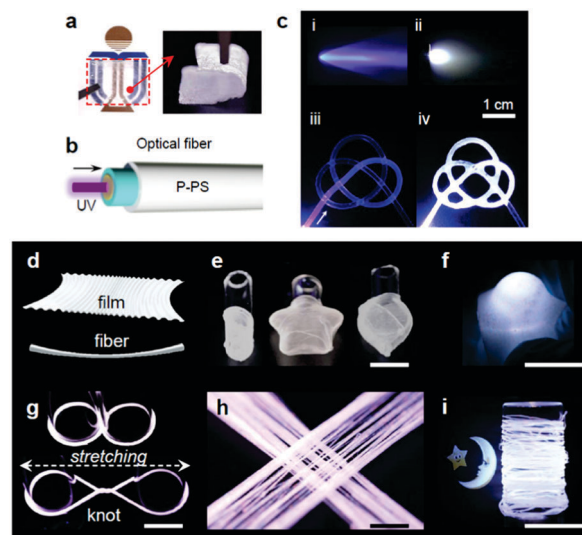


**Fig. 4** White light-emitting materials. (a) (left) Image of flexible transparent P-PS films ( $2.5 \times 3.5$  cm) taken under day light. The dotted line indicates the boundary of the film. (right) Fluorescent images of bendable P-PS film taken under 365 nm UV light irradiation. (b) Schematic image of the optical fiber coated with P-PS. (c) Photographs of (i and ii) UV LED flashlight and (iii and iv) flexible 1D optical fibers (i and iii) before and (ii and iv) after being coated with P-PS film. (d) Schematic illustration of T-SB in the forms of stretchable film and fiber. (e) Fluorescent images of T-SB films with various irregular shapes. (f) Photograph of T-SB elastic film deposited on a glass shade integrated with 365 nm UV LED. (g) Fluorescent images of T-SB-based stretchable 1D yarns fabricated by the wet-spinning process. The elastic yarns can be wound onto a substrate or knotted into various forms. (h) Fluorescent image of T-SB-based 2D fabrics taken under 365 nm UV light. (i) Pictures of T-SB-based 3D white lights integrated with 365 nm UV LED. The scale bars are 2 cm.

1D optical fiber (Fig. 4c(iii and iv)) and bright-white fluorescence was observed upon illumination with 365 nm radiation from one end of the optical fiber. It is worth noting that the good processability of P-PS provides the possibility of using various substrates for lighting. In addition, the utilization of commercial material hosts can be easily scaled up to the desired levels.

Stretchable light-emitting materials enable applications ranging from artificial skins and soft robotics to wearable technology.<sup>6</sup> As shown in Fig. 4d (top) for the schematic illustration, a highly stretchable film of T-SB was formed by drop-casting, thanks to the elastomeric nature of SB. The ductile T-SB film with a strain of  $\sim 350\%$  is compliant with curved or dynamic surfaces (Fig. S8, ESI<sup>†</sup>). With this outstanding deformability, T-SB can be seamlessly integrated on transparent glass shades of various curvatures (*e.g.*, tube, star and heart shape), as shown in Fig. 4e. A T-SB film was simply wrapped around glass shades followed by integration with a UV LED to achieve white light (Fig. 4f). Wet spinning technique was applied to eject the spinning dope to a coagulation bath (ethanol) to generate continuous T-SB fibers (Fig. S9, ESI<sup>†</sup>). These elastic fibers (Fig. 4d, bottom) can be wound onto a substrate or knotted into various forms (Fig. 4g). They can be stretched up to 580% of their original length without obvious structural change (Fig. S8, ESI<sup>†</sup>). A unique advantage of our stretchable T-SB fibers is to directly build a textile or fabric with diverse structures for lighting (Fig. 4h and i). Therefore, these continuous and stretchable fibers provide an approach to generate hierarchical white light-emitting materials with useful structures suitable for integration with fabrics to produce smart apparel.

### White CPL generation

In nature, chirality is found in diverse biological structures, such as  $\alpha$ -helical proteins, double-helical DNA and triple-helical peptides, and is responsible for their sophisticated functions.<sup>42</sup> Circularly polarized light (CPL) has been considered as a type of energy that contains chiral information and may be a prerequisite for the origin of life.<sup>43</sup> To realize CPL of materials, especially in achiral ones, artificial chiral-organization hosts have been demonstrated to divide incident light into two CPL components by selective reflection and transmission modulated by their helical sense.<sup>33,44,45</sup> As mentioned above, white-emissive materials have already been demonstrated by tuning the compositions of AIE crystalline and amorphous nano-aggregates in the polymer matrix. If helical organization was further introduced into these composites, white CPL would be ultimately generated. The ability of poly(L-lactide) (PLLA) to spontaneously form helical assemblies with twisted lamellae along the radial growth direction makes it an ideal candidate as a chiral host.<sup>35</sup> Because PLLA ( $T_g = 63\text{ }^\circ\text{C}$ ) shows a comparable rigidity with that of PS ( $T_g = 89\text{ }^\circ\text{C}$ ), PDHA was selected to interact with PLLA (Fig. S2, ESI<sup>†</sup>). The hypothetical mechanism of white CPL generation of achiral PDHA is illustrated. In Fig. 5a, as crystallization occurs upon slow solution evaporation, the helical PLLA chains fold into crystalline lamellae and exclude the PDHA molecules from the amorphous region between lamellae. Both amorphous and crystalline PDHA nano-aggregates are then formed to induce the white light emission. During the

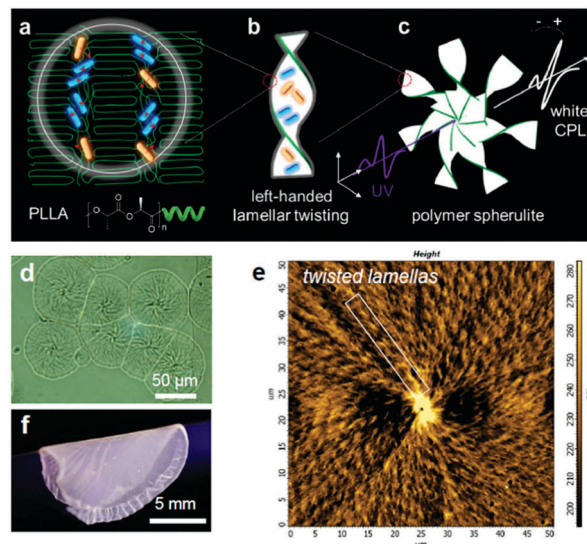
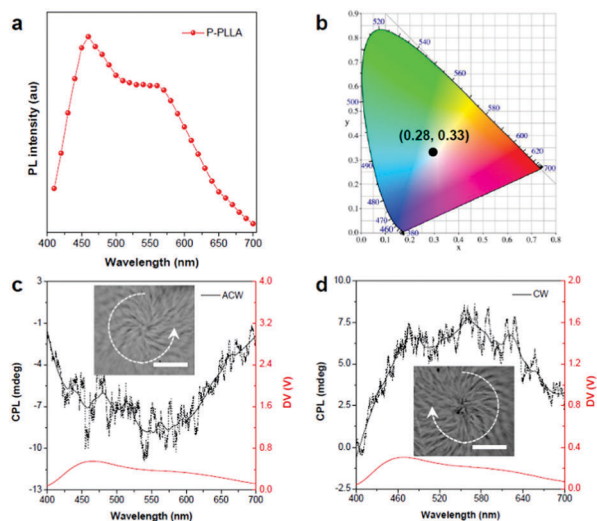


Fig. 5 Intrinsic CPL ability of polymer matrix. (a–c) Illustration of the formation of 3D spiral banded spherulite doped with PDHA nano-aggregates and the hypothetical mechanism of CPL generation. (a) Packing of PDHA aggregates with white emission in the amorphous region between polymer crystalline lamellae. (b) PDHA-c and PDHA-am aggregates on the surface of twisted lamellae. (c) Polymer spherulite with spiral structure developed from the radial growth of the twisted lamellae acts as chiral medium to generate CPL by preferential reflection of the co-handed CPL. (d) Bright-field microscopic image of spiral spherulites of P-PLLA. (e) AFM topography of polymer spherulites of P-PLLA. (f) Fluorescent image of flexible crystalline P-PLLA film taken under 365 UV light excitation.

radial growth of the spherulites, left-handed lamellar twisting appears owing to the imbalanced stress at the opposite folding surfaces (Fig. 5b).<sup>46</sup> Eventually, a spherulite with a helical superstructure will be produced. Such polymeric chiral structures with helical sense have an intrinsic ability for CPL modulation upon UV excitation (Fig. 5c). The microscopic images given in Fig. 5d show the formation of spherulites with anticlockwise spirals during the polymer crystallization process (Fig. S10, ESI<sup>†</sup>). Such asymmetric morphology is attributed to the non-diametric sections of 3D spherulites.<sup>47</sup> Both Maltese cross and extinction bands are identified under the polarized optical microscope (Fig. S11, ESI<sup>†</sup>). The helical microstructure of PDHA-embedded PLLA films (abbreviated as P-PLLA) was further verified by atomic force microscopic (AFM) analysis. The ridge-to-valley height difference can be clearly observed in the marked area of Fig. 5e, which originates from the periodic twisting of lamellae (Fig. S12, ESI<sup>†</sup>).<sup>48</sup> Finally, a flexible and continuous white-emissive film under UV excitation was generated as the polymer crystallization completed (Fig. 5f).

From the PL of P-PLLA, as shown in Fig. 6a, dual emission bands corresponding to those of PDHA-c and PDHA-am are clearly observed. It is noted that the blue-to-yellow intensity ratio is increased compared with that of P-PS, which is attributed to the lower rigidity of PLLA compared with that of the PS matrix (Fig. S2, ESI<sup>†</sup>). The CIE chromaticity coordinates of P-PLLA are (0.28, 0.33) (Fig. 6b). In order to demonstrate CPL generation from spiral P-PLLA film, CPL spectroscopy was applied to study



**Fig. 6** White circularly polarized light. (a) PL spectrum of P-PLLA. Excitation wavelength: 370 nm. (b) CIE 1931 coordinates in CIE-1931 chromaticity diagram of white emissive P-PLLA. (c and d) Enantiomeric CPL switch upon P-PLLA film inversion. Insets are the bright-field microscope images of 3D spiral patterns of spiral spherulites observed from two different sides. Scale bars are 30  $\mu\text{m}$ .

the chiroptical properties. In Fig. 6c, a negative CPL response covering 400–700 nm with  $g_{\text{lum}}$  of  $\sim -2.0 \times 10^{-3}$  was detected. The asymmetric morphology of 3D spiral spherulites inspired us to invert the film sample; as a result, a positive CPL response with  $g_{\text{lum}}$  of  $\sim 2.0 \times 10^{-3}$  was obtained (Fig. 6d). It is hypothesized that the handedness reversal by a single polymeric film is selective reflection of the divided CPL components, which is modulated by the spiral morphology of spherulites, as shown in the insets (Fig. 6c and d). As a control, the P-PLLA composite film without spiral morphology (that is, “amorphous” polymer matrix) was also prepared by rapid evaporation from solution. In this case, the “amorphous” PLLA polymer chains were randomly distributed rather than ordered organization in the crystalline spherulites, which can be demonstrated by the microscopic images (Fig. S11, ESI<sup>†</sup>). By contrast, for “amorphous” P-PLLA, the CPL spectrum is silent (Fig. S13, ESI<sup>†</sup>). Although P-PLLA films in both polymeric “crystalline” and “amorphous” forms show CD signals in the absorption region of PDHA (Fig. S11, ESI<sup>†</sup>), this could not explain why the same “crystalline” film of P-PLLA emits CPL of the opposite sense or why the “amorphous” film shows no CPL response. Therefore, the CPL is more likely to originate from the microscopic polymer superstructure rather than molecular chirality transfer. These results indicate that the CPL response is sensitive to the handedness of the spiral patterns of the polymer composites, and enantiomeric CPL switching is successfully realized (Fig. S14, ESI<sup>†</sup>). The PLLA macroscopic film with superstructures clearly provides a simple and low-cost approach for fabricating circularly polarized white-emissive materials with deformability.

We believe that the approach is not limited to the polymers and processing methods mentioned above. It has been demonstrated that a crystalline polymer with a lamellar twisting

microstructure is critical for CPL generation. Some polymers with a helical microstructure, like poly(D-lactic acid), poly(propylene oxide), and poly(epichlorohydrin), are all promising candidates for inducing CPL.<sup>49</sup> At the same time, by controlling the interactions between guest molecules and host polymers as well as the helical microstructure of polymers, the optimization of the dissymmetry factor ( $|g_{\text{lum}}|$ ) can be achieved. Furthermore, it is intriguing that luminescent molecules can serve as built-in sensors for future studies to deepen the fundamental understanding of the polymer manufacturing process when solidified from solutions or melts.<sup>50,51</sup>

## Conclusions

In summary, we presented a strategy that is adapted from methods to control bulk-commodity polymers to modulate the organization of AIE crystalline and amorphous nano-aggregates in a polymer matrix with a tailored microstructure. This path opens new capabilities for processing and structural control of luminescent molecules to generate versatile fluorescence that is beyond their intrinsic emissions, including tunable emission color, white-light emission and white CPL. A critical feature of this strategy is that it is simply and widely applicable to other organic molecules and also endows the resulting materials with softness and deformability. The resulting materials readily form films or fibers for devices with diverse configurations as well as excellent flexibility and stretchability for multiple applications. Complex hierarchical organizations of AIEgens can be built rapidly to realize tunable emission without tedious organic synthesis by simply mixing AIEgens with commercially available polymers. We envision that the present strategy for constructing emissive materials will open numerous opportunities for applications in flexible devices and wearable systems. Future work will further exploit the novel polymer micropattern control to improve the capability for emission modulation.

## Conflicts of interest

There are no conflicts to declare.

## Acknowledgements

This work was partially supported by the National Science Foundation of China (51603035, 51703042, 51508242, 21788102, 21490570 and 21490574), the Research Grants Council of Hong Kong (16308016, 16308116, C2014-15G, C6009-17G, N-HKUST604/14 and A-HKUST605/16), the Innovation and Technology Commission (ITC-CNRC14SC01 and ITS/254/17), the Science and Technology Plan of Shenzhen (JCYJ20170811155015918, JCYJ20170818113602462, JCYJ2016-0229205601482 and JCYJ20160509170535223), Science and Technology Commission of Shanghai Municipality (16JC1400700, 17ZR1446300), the China Postdoctoral Science Foundation (2016M591572 and 2017T100256), the Fundamental Research Funds for the Central Universities (2232018D3-01), and State

Key Laboratory for Modification of Chemical Fibers and Polymer Materials, Donghua University.

## Notes and references

- S. S. Babu, M. J. Hollamby, J. Aimi, H. Ozawa, A. Saeki, S. Seki, K. Kobayashi, K. Hagiwara, M. Yoshizawa, H. Möhwald and T. Nakanishi, *Nat. Commun.*, 2013, **4**, 1969.
- L. Maggini and D. Bonifazi, *Chem. Soc. Rev.*, 2012, **41**, 211.
- D. Yin, J. Feng, R. Ma, Y. F. Liu, Y. L. Zhang, X. L. Zhang, Y. G. Bi, Q. D. Chen and H. B. Sun, *Nat. Commun.*, 2016, **7**, 11573.
- M. S. White, M. Kaltenbrunner, E. D. Glowacki, K. Gutnichenko, G. Kettlgruber, I. Graz, S. Aazou, C. Ulbricht, D. A. M. Egbe, M. C. Miron, Z. Major, M. C. Scharber, T. Sekitani, T. Someya, S. Bauer and N. S. Sariciftci, *Nat. Photonics*, 2013, **7**, 811.
- Z. Zhang, L. Cui, X. Shi, X. Tian, D. Wang, C. Gu, E. Chen, X. Cheng, Y. Xu, Y. Hu, J. Zhang, L. Zhou, H. H. Fong, P. Ma, G. Jiang, X. Sun, B. Zhang and H. Peng, *Adv. Mater.*, 2018, **30**, 1800323.
- C. Larson, B. Peele, S. Li, S. Robinson, M. Totaro, L. Beccai, B. Mazzolai and R. Shepherd, *Science*, 2016, **351**, 1071.
- M. Vosgueritchian, J. B. H. Tok and Z. Bao, *Nat. Photonics*, 2013, **7**, 769.
- J. Liang, L. Li, X. Niu, Z. Yu and Q. Pei, *Nat. Photonics*, 2013, **7**, 817.
- W. Kazuyoshi and A. Kazuo, *Sci. Technol. Adv. Mater.*, 2014, **15**, 044203.
- Y. Kubo and R. Nishiyabu, *Polymer*, 2017, **128**, 257.
- R. Hanlon, *Curr. Biol.*, 2007, **17**, R400.
- L. M. Mäthger, E. J. Denton, N. J. Marshall and R. T. Hanlon, *J. R. Soc., Interface*, 2009, **6**, S149.
- H. Wynberg, E. W. Meijer, J. C. Hummelen, H. P. J. M. Dekkers, P. H. Schippers and A. D. Carlson, *Nature*, 1980, **286**, 641.
- F. Ciardelli, G. Ruggeri and A. Pucci, *Chem. Soc. Rev.*, 2013, **42**, 857.
- A. Pucci, R. Bizzarri and G. Ruggeri, *Soft Matter*, 2011, **7**, 3689.
- R. J. Wojtecki, M. A. Meador and S. J. Rowan, *Nat. Mater.*, 2011, **10**, 14.
- C. Löwe and C. Weder, *Adv. Mater.*, 2002, **14**, 1625.
- A. Lavrenova, D. W. R. Balkenende, Y. Sagara, S. Schrettl, Y. C. Simon and C. Weder, *J. Am. Chem. Soc.*, 2017, **139**, 4302.
- C. Calvino, A. Guha, C. Weder and S. Schrettl, *Adv. Mater.*, 2018, **30**, 1704603.
- B. R. Crenshaw and C. Weder, *Macromolecules*, 2006, **39**, 9581.
- B. R. Crenshaw, M. Burnworth, D. Khariwala, A. Hiltner, P. T. Mather, R. Simha and C. Weder, *Macromolecules*, 2007, **40**, 2400.
- M. Kinami, B. R. Crenshaw and C. Weder, *Chem. Mater.*, 2006, **18**, 946.
- J. Mei, N. L. C. Leung, R. T. K. Kwok, J. W. Y. Lam and B. Z. Tang, *Chem. Rev.*, 2015, **115**, 11718.
- W. Z. Yuan, Y. Tan, Y. Gong, P. Lu, J. W. Y. Lam, X. Y. Shen, C. Feng, H. H. Y. Sung, Y. Lu, I. D. Williams, J. Z. Sun, Y. Zhang and B. Z. Tang, *Adv. Mater.*, 2013, **25**, 2837.
- N. Zhao, M. Li, Y. Yan, J. W. Y. Lam, Y. L. Zhang, Y. S. Zhao, K. S. Wong and B. Z. Tang, *J. Mater. Chem. C*, 2013, **1**, 4640.
- Z. He, L. Zhang, J. Mei, T. Zhang, J. W. Y. Lam, Z. Shuai, Y. Q. Dong and B. Z. Tang, *Chem. Mater.*, 2015, **27**, 6601.
- Y. Hong, J. W. Y. Lam and B. Z. Tang, *Chem. Commun.*, 2009, 4332.
- Y. Cheng, J. Wang, Z. Qiu, X. Zheng, N. L. C. Leung, J. W. Y. Lam and B. Z. Tang, *Adv. Mater.*, 2017, **29**, 1703900.
- T. Han, C. Gui, J. W. Y. Lam, M. Jiang, N. Xie, R. T. K. Kwok and B. Z. Tang, *Macromolecules*, 2017, **50**, 5807.
- S. H. Chen, D. Katsis, A. W. Schmid, J. C. Mastrangelo, T. Tsutsui and T. N. Blanton, *Nature*, 1999, **397**, 506.
- M. Liu, L. Zhang and T. Wang, *Chem. Rev.*, 2015, **115**, 7304.
- J. Kumar, T. Nakashima and T. Kawai, *J. Phys. Chem. Lett.*, 2015, **6**, 3445.
- H. Zheng, W. Li, W. Li, X. Wang, Z. Tang, S. X. A. Zhang and Y. Xu, *Adv. Mater.*, 2018, **30**, 1705948.
- T. Wen, H. F. Wang, M. C. Li and R. M. Ho, *Acc. Chem. Res.*, 2017, **50**, 1011.
- M. C. Li, H. F. Wang, C. H. Chiang, Y. D. Lee and R. M. Ho, *Angew. Chem., Int. Ed.*, 2014, **53**, 4450.
- H. Zhang, X. Zheng, N. Xie, Z. He, J. Liu, N. L. C. Leung, Y. Niu, X. Huang, K. S. Wong, R. T. K. Kwok, H. H. Y. Sung, I. D. Williams, A. Qin, J. W. Y. Lam and B. Z. Tang, *J. Am. Chem. Soc.*, 2017, **139**, 16264.
- Z. He, W. Zhao, J. W. Y. Lam, Q. Peng, H. Ma, G. Liang, Z. Shuai and B. Z. Tang, *Nat. Commun.*, 2017, **8**, 416.
- G. Iasilli, A. Battisti, F. Tantussi, F. Fuso, M. Allegrini, G. Ruggeri and A. Pucci, *Macromol. Chem. Phys.*, 2014, **215**, 499.
- R. M. Dammert, S. L. Maunu, F. H. J. Maurer, I. M. Neelov, S. Niemelä, F. Sundholm and C. Wästlund, *Macromolecules*, 1999, **32**, 1930.
- G. Strobl, *The Physics of Polymers, Concepts for Understanding Their Structures and Behavior*, Springer, Berlin, Germany, 2007.
- K. V. Rao, K. K. R. Datta, M. Eswaramoorthy and S. J. George, *Adv. Mater.*, 2013, **25**, 1713.
- D. Yang, P. Duan, L. Zhang and M. Liu, *Nat. Commun.*, 2017, **8**, 15727.
- J. Bailey, A. Chrysostomou, J. H. Hough, T. M. Gledhill, A. McCall, S. Clark, F. Ménard and M. Tamura, *Science*, 1998, **281**, 672.
- T. Kan, A. Isozaki, N. Kanda, N. Nemoto, K. Konishi, H. Takahashi, M. Kuwata-Gonokami, K. Matsumoto and I. Shimoyama, *Nat. Commun.*, 2015, **6**, 8422.
- N. Kanda, K. Konishi and M. Kuwata-Gonokami, *Opt. Lett.*, 2014, **39**, 3274.
- H. F. Wang, C. H. Chiang, W. C. Hsu, T. Wen, W. T. Chuang, B. Lotz, M. C. Li and R. M. Ho, *Macromolecules*, 2017, **50**, 5466.
- Y. Li, L. Wu, C. He, Z. Wang and T. He, *CrystEngComm*, 2017, **19**, 1210.
- J. Xu, B. H. Guo, Z. M. Zhang, J. J. Zhou, Y. Jiang, S. Yan, L. Li, Q. Wu, G. Q. Chen and J. M. Schultz, *Macromolecules*, 2004, **37**, 4118.
- B. Crist and J. M. Schultz, *Prog. Polym. Sci.*, 2016, **56**, 1.
- Z. Wang, J. Nie, W. Qin, Q. Hu and B. Z. Tang, *Nat. Commun.*, 2016, **7**, 12033.
- W. Guan, S. Wang, C. Lu and B. Z. Tang, *Nat. Commun.*, 2016, **7**, 11811.